Boundary-Layer Meteorol (2007) 122:217–241
DOI 10.1007/s10546-006-9088-y

ORIGINAL ARTICLE

A matrix approach coupled with Monte Carlo Techniques for solving the net radiative balance of the urban block

Marta J. N. Oliveira Panão · Helder J. P. Gonçalves · Paulo M. C. Ferrão

Received: 22 November 2005 / Accepted: 19 April 2006 /
Published online: 8 July 2006

Abstract A new method is developed for solving the shortwave and longwave net radiative balance of a three-dimensional urban structure, represented by parallelepiped blocks uniformly distributed in each direction. The method is based on a novel approach to determine the shape factors among surfaces, which are estimated by Monte Carlo techniques due to the complex geometry associated with the three-dimensional urban structure. Then, a set of linear equations is solved to quantify the radiative balance, in order to obtain their exact solution, considering all the inter-reflections among surfaces. The comparison between the new and the ray-tracing tracking methods resulted in a Pearson correlation coefficient of 0.996. However, by integrating the linear equations' exact solution with Monte Carlo techniques, the new method reduces by a factor of 36 the central processing unit (CPU) time used to perform the calculations of the ray-tracing tracking method. The use of the model for a sensitivity study allows us to verify the effective absorptance and emittance increases with the canyon aspect ratio of the urban layout. An urban structure formed by square cross-sectional blocks absorbs more solar radiation than an urban structure formed by rectangular cross-sectional blocks. The approximation of a specific geometry for an equivalent bi-dimensional infinite street can be applied for rectangular cross-sectional blocks, where the width is 11 times or more greater than the depth dimension.

Keywords Monte Carlo · Multiple reflections · Radiative balance · Three-dimensional geometry · Urban longwave matrix · Urban shortwave matrix

M. J. N. Oliveira Panão (✉) · H. J. P. Gonçalves
Renewable Energy Department,
National Institute of Engineering, Technology and Innovation (INETI),
Estrada do Paço do Lumiar 22, 1649-038 Lisbon, Portugal
e-mail: marta.oliveira@ineti.pt

P. M. C. Ferrão
IN+, Center for Innovation, Technology and Policy Research
Instituto Superior Técnico, Av. Rovisco Pais,
1049-001 Lisbon, Portugal

List of Symbols

a, b, c, d	wall building surfaces
f	fraction of rays which intersect the surface
h	altitude above sea (km)
l	proportion between block width and depth
m	total number of surfaces
n	number of neighbour urban units
n_{it}	number of iterations
n_{sb}	number of sub-surfaces
k	number of subdivisions of a vertical surface
r	number of grid nodes
r_{se}	sun–earth distance factor
z	zenith angle (rad)
A	surface area (m^2)
$\mathbf{A}, \mathbf{A}_1, \mathbf{A}_2$	absorptivity matrices
B	total outgoing radiative flux density ($\mathrm{W\,m^{-2}}$)
$\mathbf{B}$	total outgoing radiative flux density vector ($\mathrm{W\,m^{-2}}$)
D	horizontal sky diffuse radiation flux density ($\mathrm{W\,m^{-2}}$)
$\mathbf{E}, \mathbf{E}_1$	emissivity matrices
F	shape factor between surfaces
$\mathbf{F}$	shape factor matrix
G	global radiation flux density ($\mathrm{W\,m^{-2}}$)
H	building block height (m)
$\mathbf{I}$	identity matrix
J_{day}	Julian day
I_0	solar constant ($\mathrm{W\,m^{-2}}$)
K	direct surface irradiation flux density ($\mathrm{W\,m^{-2}}$)
$K_\perp$	normal direct radiation flux density ($\mathrm{W\,m^{-2}}$)
$L_\downarrow$	sky downward longwave radiative flux density ($\mathrm{W\,m^{-2}}$)
L	building block width (m)
M	air mass (kg)
W	space between blocks (m)
T	absolute temperature (K)
T_{L}	Linke turbidity factor
α	absorptance
$\boldsymbol{\alpha}$	absorptivity vector
δ	layout azimuth (deg)
ε	emittance
$\boldsymbol{\varepsilon}$	emissivity vector
$\boldsymbol{\kappa}$	Ψ weighting area vector
ρ	Pearson correlation coefficient
σ	Stephan–Boltzman constant ($\mathrm{W\,m^{-2}K^{-4}}$)
$\boldsymbol{\omega}$	Ω normalized vector
Φ	surface net radiative flux density ($\mathrm{W\,m^{-2}}$)
$\boldsymbol{\Phi}$	net radiative flux vector ($\mathrm{W\,m^{-2}}$)

Γ	transformation matrix
Λ	total incoming radiative flux density ($\mathrm{W\,m^{-2}}$)
$\mathbf{\Omega}_\mathrm{L}$	black surface emitted radiation vector ($\mathrm{W\,m^{-2}}$)
$\mathbf{\Omega}_\mathrm{S}$	shortwave irradiation vector ($\mathrm{W\,m^{-2}}$)
Ψ	urban matrix

Subscripts

i, j	general surfaces indexes
g	ground surface
rf	roof surface
sf	generic surface
ub	urban block
w	wall surface
wg	walls and ground surfaces
x, y	x- and y-axis
S	shortwave
L	longwave

1 Introduction

Modelling heat transfer processes in urban canyons has for long been studied either experimentally or numerically (Nunez and Oke 1977; Yoshida et al. 1990–91; Arnfield 1982; Mills 1993; Kobayashi and Takamura 1994; Sakakibara 1996; Mason 2000; Kusaka et al. 2001; Martilli et al. 2002). The three-dimensionality of urban structures is often simplified into an urban canyon configuration, i.e., there is a two-dimensional (2D) cut of a long street formed by two opposite building walls and the surface between them. This geometry, the urban canyon, has been extensively studied as it is considered to be a fundamental morphological unit that forms city blocks, neighbourhoods or even the entire city (Arnfield 2003). However, the extrapolation of urban canyon (2D) to a three-dimensional urban layout (3D) is a rough estimation of radiative exchanges (Arnfield 1988).

Few studies propose 3D models for calculating radiative exchanges among surfaces. On the one hand, Kanda et al. (2005) developed a scheme to calculate these exchanges without time-consuming processes, but the model only applies to regular urban structures, formed by buildings with a square horizontal cross-section, equally spaced on both directions. Kondo et al. (2001), Kawai and Kanda (2003) and Chimklai et al. (2004) have, otherwise, used the Monte Carlo approach by photon or vector tracking methods, which is particularly adapted for complex geometries, although computationally slow, due to the large number of iterations required. On the other hand, radiative exchanges among surfaces are intrinsically related to shape-factor geometry, and once the shape factors are determined, Sparrow and Cess (1978) proposed to solve algebraically a set of linear equations to evaluate the radiative fluxes (enclosure radiosity method). However, such methodology was applied only for an enclosure space with a courtyard form (Verseghy and Munro 1989a, b) and a 2D urban canyon (Swaid 1993; Pawlak and Fortuniak 2002, 2003; Harman et al. 2004).

In our study, the enclosure radiosity method used to determine radiative exchange is combined with Monte Carlo techniques for shape-factor calculation, resulting in a new and expedited method to solve radiative exchanges among surfaces in a 3D urban layout, formed by buildings with a rectangle horizontal cross-section, equally spaced in each direction although independently, provided that a set of requirements is satisfied, as discussed in Sect. 2. The method is described in Sect. 3, and then it is applied to calculate the effective absorptance and emittance of an urban structure (Sect. 4). Further, it is shown that the new method, run with sufficient spatial resolution and a minimum number of iterations, provides an excellent agreement with the ray-tracing method (Sect. 5) and experimental data from Aida (1982) (Sect. 6). In Sect. 7, a sensitivity study is performed to analyze the influence on the net effect of the urban structure of the canyon aspect ratio and different layouts, such as square and rectangular cross-sectional blocks, as well as streets.

2 Radiosity method requirements

The methodology for solving the radiative exchanges among surfaces in a 3D model of an urban environment, as depicted in Fig. 1, is based on the exact solution proposed by Sparrow and Cess (1978) for diffuse irradiance exchanges among surfaces of an enclosure space, hereafter designated by RAM (radiosity method). According to Sparrow and Cess (1978), RAM is valid for a defined enclosure if: (i) each surface is grey and isothermal; (ii) reflected and emitted radiation is diffusely distributed; (iii) the irradiance is constant along the surfaces; and (iv) the intervening medium does not absorb or emit radiation. Therefore, the difficulty in applying RAM to a 3D urban environment is fivefold: (1) the urban environment is not closed, (2) building surfaces are neither grey nor isothermal, (3) there are surfaces that are specular reflectors of solar radiation, (4) irradiance is not constant along surfaces because of shadow patterns, and (5) the air is not transparent to specific wavelength radiation ranges. In the following subsections, an explanation is presented on how the newly developed method overcomes these limitations, except for specular reflections, which were not considered.

2.1 Urban enclosure

The geometry of the model is a regular urban structure defined by five variables (Fig. 1). Three of them refer to the building block width (L_x), depth (L_y) and height (H). The several blocks are uniformly spaced on the x-axis by W_x and on

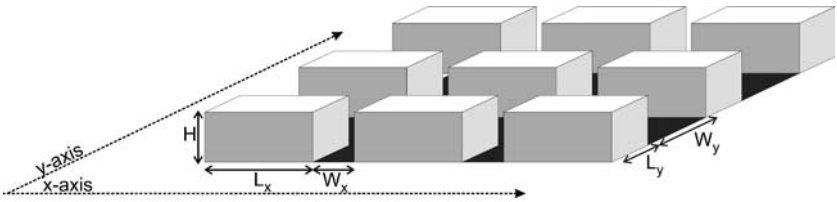

Fig. 1 Urban geometry

Fig. 2 Urban layout azimuth

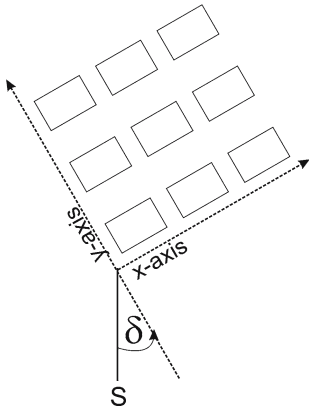

Fig. 3 Building block (A) and urban canopy layer (B)

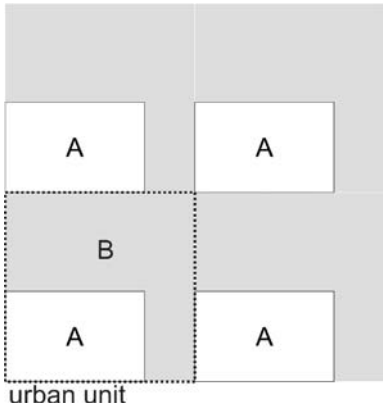

the y-axis by W_y. The layout azimuth (δ) is defined by the angle between the negative direction on the y-axis and the south, as depicted in Fig. 2. The urban unit, which is repeated throughout the entire domain, is composed of the building block itself (A in Fig. 3) and the air volume in the space within blocks (B in Fig. 3).

The urban enclosure is the entire grid formed by a large, but finite, number of urban units (n). Therefore, the shape factors between surfaces are not restricted to the surfaces inside the urban unit. The shape factor between surfaces c and d, $F_{c\to d}$, is defined as the fraction of surfaces d within the entire vision field of surface c. In this example, c "sees" $d, d_1, d_2, \ldots, d_n$ (Fig. 4), and therefore $F_{c\to d}$ is calculated as the area of all the surfaces of type d, divided by the area that corresponds to the vision field of surface c, as represented in Fig. 5 (medium grey). Another example considers that, even if the c surface does not "see" b inside the urban unit, the shape factor $F_{c\to b}$ is not null because c "sees" $b_1, b_2, \ldots, b_n$ (dark grey in Fig. 5). It should be noted that the surface numerical index $(1, 2, \ldots, n)$ indicates how many urban units a fictitious ray from the main unit has to cross to reach that surface (Fig. 4). The differentiation of surfaces by orientation (a, b, c and d) even outside the urban unit is related to their exposure to the solar radiation. For example, the surface b irradiance is equal to that of surface b_1 or b_2 (Fig. 4) because all surfaces of the same type have the same geometrical position relative to the others remaining.

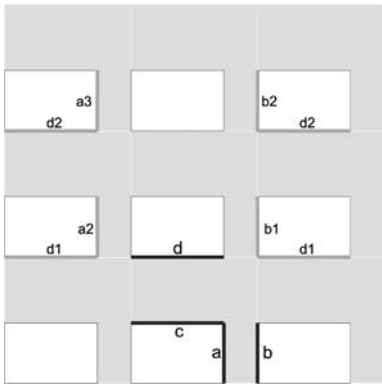

Fig. 4 Shape-factor geometry

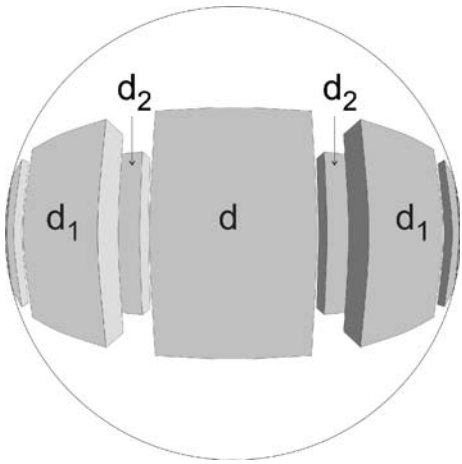

Fig. 5 Fish-eye view at midpoint of surface *c*. Surface *d* medium grey, surface *a* light grey, surface *b* dark grey. Sky and ground surfaces are represented as white

The term 'shape factor' is applied instead of 'view factor' in order to express the relation between two non-infinitesimal surfaces. In fact, Johnson and Watson (1984) and Steyn and Lyons (1985) showed that there is a large variation of view factor (infinitesimal surface to surface view factor) with the position on the surface, justifying this differentiation.

2.2 Selective grey surfaces

For grey surfaces, the emissivity and absorptivity properties are independent of wavelength and, according to Kirchhoff's law, the emissivity can be assumed equal to absorptivity. However, building surfaces are not physically grey, but can be treated as selective grey surfaces (Athienitis and Santamouris 2002). Therefore, the above assumptions are valid only for a specific wavelength range. In the case of building modelling, this wavelength range is divided into "shortwave" and "longwave", i.e., below and above $3\,\mu$m, respectively. In fact, 99% of the incoming solar radiation is within the shortwave range (shortwave radiation). Otherwise, depending on the range of temperatures of building surfaces, the radiation wavelength that is emitted is within the longwave range (longwave radiation). Because building surfaces are

selective, the radiative processes can be treated independently on each one of the two ranges (Sparrow and Cess 1978).

This model assumes that air is a non-participating medium as RAM requires, however, the air is not transparent to longwave radiation, due to the water vapor and CO_2 emission and absorption bands above 2.7 μm. Verseghy and Munro (1989b) showed that neglecting this effect causes an error as the same order of magnitude as their model.

In the new method, different absorptivity and emissivity values for surfaces with different orientations are allowed, i.e., the properties of surface *a* (Fig. 4) can be different from those of surface *b*, *c* or *d*; however all surfaces of type *a* ($a_1, a_2, \ldots, a_n$) should have the same properties. Consequently, even if the geometry of the model is symmetrical, the layout azimuth can vary between 0° and 360°, in order to allow different azimuth angles to each one of the surfaces.

2.3 The number of surfaces

The error introduced by assuming a constant irradiance throughout the surface is minimized if the vertical surfaces are divided into *k* parcels. The total number of surfaces is *m*, which equals $4k + 4$; $4k$ is the number of vertical subsurfaces and 4 is the number of the ground and sky surfaces. Surface *a* indices are illustrated in Fig. 6a; the ground and sky surfaces indices are illustrated in Fig. 6b, c, respectively. Surfaces *b*, *c* and *d* indices are similarly distributed as in surface *a*, but start at $k+1$, $2k+1$ and $3k + 1$, respectively. As for different types of surfaces, surfaces with different positions can have different emissivity and absorptivity properties. And, finally, thermal differences between surfaces are also minimized with this division procedure, because surface temperature is strictly related to irradiance levels and air-induced horizontal and vertical gradients (Santamouris 2001).

3 Radiosity method coupled with Monte Carlo techniques (RAM-MC)

3.1 The shape-factor matrix (**F**)

Shortwave and longwave radiative exchanges among surfaces are intrinsically dependent on shape-factor geometry (Arnfield, 1982; Harman et al. 2004; Kanda et al. 2005). In order to build the shape-factor matrix, **F**, where each term $F_{i,j}$ is the shape factor between surface *i* and *j*, $F_{i\rightarrow j}$, an iterative method based on Monte Carlo techniques was developed: see Appendix 1 for more details. It should be noted that the reciprocity rule cannot be applied because the surface *i* is within the urban unit, but surface *j* includes all the surfaces of the same type in the enclosure. The process is optimized, however, by considering surfaces *a* and *c* with geometrical positions identical to surfaces *b* and *d*, respectively. The process is also valid within each surface type (a, b, c, d); for example, the surface 1 in Fig. 6a has an inverse geometrical position relative to the surface *k*.

For the geometry in Fig. 1, considering the surface indices defined in Fig. 6, **F** takes the generic matrix form of:

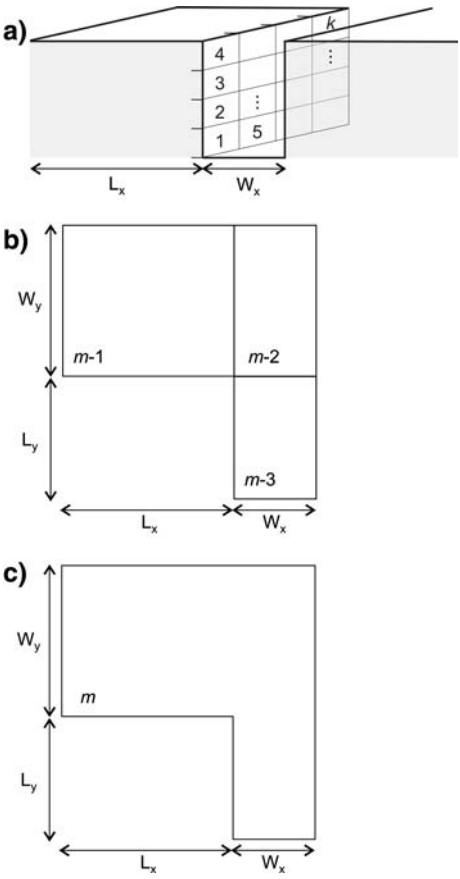

Fig. 6 Surfaces indexes: (**a**) vertical, (**b**) ground and (**c**) sky surfaces

$$\mathbf{F} = \begin{pmatrix} 0 & F_{1,2} & \cdots & F_{1,4k} & F_{1,m-3} & F_{1,m-2} & F_{1,m-1} & F_{1,m} \\ F_{2,1} & 0 & \cdots & F_{2,4k} & F_{2,m-3} & F_{2,m-2} & F_{2,m-1} & F_{2,m} \\ \vdots & \vdots & \ddots & \vdots & \vdots & \vdots & \vdots & \vdots \\ F_{4k,1} & F_{4k,2} & \cdots & 0 & F_{4k,m-3} & F_{4k,m-2} & F_{4k,m-1} & F_{4k,m} \\ F_{m-3,1} & F_{m-3,2} & \cdots & F_{m-3,4k} & 0 & 0 & 0 & F_{m-3,m} \\ F_{m-2,1} & F_{m-2,2} & \cdots & F_{m-2,4k} & 0 & 0 & 0 & F_{m-2,m} \\ F_{m-1,1} & F_{m-1,2} & \cdots & F_{m-1,4k} & 0 & 0 & 0 & F_{m-1,m} \\ F_{m,1} & F_{m,2} & \cdots & F_{m,4k} & F_{m,m-3} & F_{m,m-2} & F_{m,m-1} & 0 \end{pmatrix}. \quad (1)$$

It is noteworthy that the analytical calculation of **F** is extremely difficult for the geometry depicted in Fig. 1, which is a function of five geometrical variables: L_x, L_y, W_x, W_y and H. The solution obtained by the Monte Carlo method depends on the number of iterations n_{it} (Appendix 1), number of neighbour units n and number of subdivisions of vertical surfaces k. The choice of the values for those simulation parameters is discussed in Sect. 5.

3.2 The urban longwave and shortwave matrixes for black surfaces

3.2.1 Longwave range

Considering the geometry of Fig. 1 where walls and ground are black surfaces (emissivity, ε, and absorptivity, α, are equal to 1 and the reflectivity is 0), once the shape-factor matrix is created, the net longwave radiative flux for a given surface j, Φ_j, is:

$$\Phi_j = -\Omega_{\mathrm{Lj}} + \sum_{i=1}^{m} F_{i,j}\Omega_{\mathrm{L}i} \tag{2}$$

where $\Omega_{\mathrm{L}i}$ is the net radiative flux emitted by the surface i. For surfaces $i \neq m$, $\Omega_{\mathrm{L}i}$ is σT_i^4, according to the Stephan–Boltzman law; instead, $\Omega_{\mathrm{L}m}$ is the sky downward longwave radiative flux ($L_{\downarrow}$).

The above formulation (2) can be applied to all surfaces, excluding the sky surface, by the following linear equation in its matrix form:

$$\mathbf{\Phi} = \underbrace{(\mathbf{F} - \mathbf{I})}_{\mathbf{\Psi_L}} \mathbf{\Omega_L} \tag{3}$$

where $\mathbf{\Omega}_{\mathrm{L}}$ is the vector of emitted fluxes, $\mathbf{I}$ the identity matrix and $\mathbf{F}$ the shape-factor matrix defined by (1). From (3) we may identify the urban longwave matrix, $\mathbf{\psi}_{\mathrm{L}}$, an $(m-1) \times m$ matrix obtained by removing the mth row from $\mathbf{F} - \mathbf{I}$:

$$\mathbf{\Phi} = \mathbf{\Psi_L}\mathbf{\Omega_L}. \tag{4}$$

Considering this formulation, for longwave net radiative calculations, the radiative heat balance for the geometry of Fig. 1 is characterized by the urban longwave matrix, $\mathbf{\psi}_{\mathrm{L}}$. As long as $\mathbf{\psi}_{\mathrm{L}}$ is established, if the surface temperature changes, new $\mathbf{\Omega}_{\mathrm{L}}$ and net radiative balance $\mathbf{\Phi}$ vectors are directly computed.

3.2.2 Shortwave range

The calculation of net shortwave radiative flux has a different formulation. Assuming that the horizontal sky diffuse radiation flux density is D and surface i is directly irradiated with the flux density K_i, because a black surface absorbs all the incident radiation, the net flux is given by

$$\Phi_i = K_i + F_{i,m}D. \tag{5}$$

As with (4), the shortwave net radiative flux can be expressed as a function of an urban shortwave matrix $\mathbf{\psi}_{\mathrm{S}}$ and $\mathbf{\Omega}_{\mathrm{S}}$ by

$$\mathbf{\Phi} = \mathbf{\Psi_S}\mathbf{\Omega_S}, \tag{6}$$

where each Ω_{Si} corresponds to K_i, for $i \neq m$, and D, for $i = m$, and $\mathbf{\psi}_{\mathrm{S}}$ is an $(m-1) \times (m-1)$ identity matrix augmented with the mth column of $\mathbf{F}$ matrix.

As with the longwave range, whenever a surface irradiance changes, new $\mathbf{\Omega}_{\mathrm{S}}$ and new net radiative balance $\mathbf{\Phi}$ vectors are obtained. No change is introduced on the $\mathbf{\psi}_{\mathrm{S}}$ matrix itself.

3.3 The urban longwave and shortwave matrixes for grey surfaces

Physically, the urban shortwave matrix, $\boldsymbol{\psi}_{\mathrm{S}}$, characterizes the distribution of solar irradiance from a specific surface to all surrounding surfaces, which, for grey surfaces, includes all the inter-reflections. For example, the irradiance of surface j is Ω_{Sj}, and is partially absorbed by the surface j, $\boldsymbol{\psi}_{Sj,j}$ and the remaining terms of the same column j, $\boldsymbol{\psi}_{Si,j}$ with $i \neq j$, are the fractions absorbed by each surface i resulting from inter-reflections. A similar explanation is associated with the urban longwave matrix $\boldsymbol{\psi}_{\mathrm{L}}$, where Ω_{Lj} is instead the equivalent flux density emitted by surface j, if the surface is black (σT_j^4).

It will be shown in the following subsections that the surface absorptivity and emissivity properties are intrinsically represented on $\boldsymbol{\psi}_{\mathrm{S}}$ and $\boldsymbol{\psi}_{\mathrm{L}}$. So, as long as these are established, Eqs. (4) and (6) are both valid for black and grey surfaces. The methodology to obtain these matrixes for grey surfaces is also discussed.

3.3.1 The urban longwave matrix $\boldsymbol{\Psi}_{\mathrm{L}}$

According to Sparrow and Cess (1978) and Harman et al. (2004) the longwave net radiative flux density for each surface is calculated from a set of equations that relates the emitted $\varepsilon_i \Omega_{\mathrm{L}i}$, total incoming Λ_i, total outgoing B_i and net Φ_i radiative flux densities by

$$\Lambda_i = \sum_{j=1}^{m} F_{i,j} B_j, \tag{7}$$

$$\mathrm{B}_i = \varepsilon_i \Omega_{\mathrm{L}i} + (1 - \varepsilon_i)\Lambda_i, \tag{8}$$

$$\Phi_i = \Lambda_i - B_i. \tag{9}$$

For the present methodology, it is assumed that each $F_{i,j}$ is known (Appendix 1) as well as each surface emitted flux $\varepsilon_i \Omega_{\mathrm{L}i}$. Moreover, Kirchhoff's law establishes for grey surfaces that α_i can be replaced by ε_i. Replacing (7) in (8) gives:

$$\mathrm{B}_i - (1 - \varepsilon_i) \sum_{j=1}^{m} F_{i,j} B_j = \varepsilon_i \Omega_{\mathrm{L}i}. \tag{10}$$

So the total outgoing longwave radiative flux of each surface, which for all surfaces corresponds to the **B** vector, can be directly obtained from the emitted radiation of each surface. The matrix form that describes the above relation is expressed by

$$\mathbf{B} = \boldsymbol{\Gamma}^{-1} \mathbf{E} \boldsymbol{\Omega}_{\mathbf{L}} \tag{11}$$

where **E** is an $m \times m$ matrix, where its diagonal terms are the emissivity surface values, such as $E_{i,i} = \varepsilon_i$, and $E_{i,j} = 0$ for $i \neq j$. The mth term, $E_{m,m}$, equivalent to emissivity of sky surface, is set to 1, because Ω_m equals $L_{\downarrow}$. $\boldsymbol{\Gamma}^{-1}$ is obtained by inverting $\boldsymbol{\Gamma}$ calculated by computing (12):

$$\boldsymbol{\Gamma} = \mathbf{I} - (\mathbf{I} - \mathbf{E})\mathbf{F}. \tag{12}$$

For surfaces with emissivity different from 1 (Sparrow and Cess 1978), the net longwave radiative flux for surface i, Φ_i, is calculated by

$$\Phi_i = \frac{\varepsilon_i}{1-\varepsilon_i}\left(\mathrm{B}_i - \Omega_{\mathrm{L}i}\right), \tag{13}$$

which, using (11), can be expressed in the matrix form:

$$\mathbf{\Phi} = \mathbf{E}_1\left(\mathbf{\Gamma}^{-1}\mathbf{E} - \mathbf{I}\right)\mathbf{\Omega_L}. \tag{14}$$

In the above expression, $\mathbf{E}_1$ is an $(m-1)\times m$ matrix:

$$\mathbf{E}_1 = \begin{pmatrix} \frac{\varepsilon_1}{1-\varepsilon_1} & 0 & \cdots & 0 & 0 \\ 0 & \frac{\varepsilon_2}{1-\varepsilon_2} & \cdots & 0 & 0 \\ \vdots & \vdots & \ddots & \vdots & \vdots \\ 0 & 0 & \cdots & \frac{\varepsilon_{m-1}}{1-\varepsilon_{m-1}} & 0 \end{pmatrix}. \tag{15}$$

Comparing (4) with (14), the $(m-1)\times m$ matrix $\mathbf{\Psi}_{\mathrm{L}}$ is then given by

$$\mathbf{\Psi_L} = \mathbf{E}_1\left(\mathbf{\Gamma}^{-1}\mathbf{E} - \mathbf{I}\right). \tag{16}$$

Besides matrix operations, obtaining the urban longwave matrix $\mathbf{\Psi}_{\mathrm{L}}$ consists mainly of, (1) the shape factor matrix estimation to obtain Γ, and (2) the Γ inversion.

3.3.2 The urban shortwave matrix $\mathbf{\Psi}_{\mathrm{S}}$

The formulation of $\mathbf{\Psi}_{\mathrm{S}}$ differs from that obtained for the urban longwave matrix, mainly because $\mathbf{\Omega}_{\mathrm{S}}$ is formed by each surface direct irradiance (1st to $m-1$th terms) and by the horizontal sky diffuse irradiance, D (mth term).

So (7) and (8) are replaced by (17) and (18) below, because the surface direct irradiance (first term of (17)) is included on the total incoming flux density and the outgoing radiation results only from the reflected fraction of the incoming, viz.

$$\Lambda_i = \Omega_{\mathrm{S}i} + \sum_{j=1}^{m} F_{i,j}B_j, \tag{17}$$

$$B_i = (1-\alpha_i)\Lambda_i. \tag{18}$$

By replacing (17) in (18), it follows that:

$$\mathrm{B}_i - (1-\alpha_i)\sum_{j=1}^{m} F_{i,j}B_j = (1-\alpha_i)\Omega_{\mathrm{S}_i}. \tag{19}$$

However, for the m surface (sky surface), this expression takes the form (20) below, obtained by considering the left side α_i term equal to 1, and the right α_i term equal to 0, viz.

$$B_m = \Omega_{\mathrm{S}_m}. \tag{20}$$

The equivalent matrix form is then:

$$\mathbf{B} = \mathbf{\Gamma}^{-1}(\mathbf{I} - \mathbf{A}_1)\mathbf{\Omega_S} \tag{21}$$

where Γ takes the same form as that obtained for longwave, replacing ε_i by α_i, which defines $\mathbf{A}$:

$$\mathbf{\Gamma} = \mathbf{I} - (\mathbf{I} - \mathbf{A})\mathbf{F}. \tag{22}$$

The $\mathbf{A}_1$ matrix is equal to $\mathbf{A}$, with the exception of the mth diagonal term, A_{mm} is 1 while $A_{1m,m}$ is 0. Combining (18) and (9) the net radiative flux is calculated from,

$$\Phi_i = \frac{\alpha_i}{1-\alpha_i} B_i. \tag{23}$$

Finally, the net radiative flux in matrix form is obtained by combining (21) with (23):

$$\mathbf{\Phi} = \mathbf{A}_2 \mathbf{\Gamma}^{-1} (\mathbf{I} - \mathbf{A}_1)\, \mathbf{\Omega_S} \tag{24}$$

where $\mathbf{A}_2$ is expressed as:

$$\mathbf{A}_2 = \begin{pmatrix} \frac{\alpha_1}{1-\alpha_1} & 0 & \cdots & 0 & 0 \\ 0 & \frac{\alpha_2}{1-\alpha_2} & \cdots & 0 & 0 \\ \vdots & \vdots & \ddots & \vdots & \vdots \\ 0 & 0 & \cdots & \frac{\alpha_{m-1}}{1-\alpha_{m-1}} & 0 \end{pmatrix}. \tag{25}$$

As with the urban longwave matrix, the main processes required to calculate $\mathbf{\Psi}_S$, given by (26), are the shape factor matrix estimation and the $\mathbf{\Gamma}$ inversion.

$$\mathbf{\Psi}_S = \mathbf{A}_2 \mathbf{\Gamma}^{-1} (\mathbf{I} - \mathbf{A}_1). \tag{26}$$

At this point it should be noted that, for the same urban geometry, the shape-factor matrix $\mathbf{F}$ is computed only once. The surface emissivity and absorptivity values determine the form of the urban longwave and shortwave matrixes, $\mathbf{\Psi}_L$ and $\mathbf{\Psi}_S$. The following section will present an application of this methodology.

4 Urban block net effect

4.1 Effective absorptance

The urban shortwave matrix approach is used to calculate the effective absorptance of an urban block, α_{ub}, i.e. the ratio between the absorbed radiation by the urban unit and the total incident radiation at its top. The physical meaning of the effective absorptance is the fraction of radiation absorbed by an equivalent surface with the same urban block area (A_{ub}) hypothetically positioned horizontally, without neighbouring surfaces causing shading or inter-reflections. The urban albedo is related to the urban absorptance by $1 - \alpha_{ub}$.

The effective absorptance of the urban block can be separated into three terms weighted by their relative areas: roof (A_{rf}), walls (A_w) and ground (A_g),

$$\alpha_{ub} = \alpha_{rf}\frac{A_{rf}}{A_{ub}} + \alpha_w \frac{A_w}{A_{ub}} + \alpha_g \frac{A_g}{A_{ub}}. \tag{27}$$

Each of these areas is given by dimensions depicted in Fig. 1, viz.

$$A_{rf} = L_x L_y, \tag{28}$$

$$A_{\mathrm{w}} = 2H(L_x + L_y), \tag{29}$$

$$A_{\mathrm{g}} = L_x W_y + L_y W_x + W_x W_y, \tag{30}$$

$$A_{\mathrm{ub}} = (L_x + W_x)(L_y + W_y). \tag{31}$$

The building height, H, of the chosen geometry is the same for all buildings and, as the roof surface irradiance is not influenced by mutual shading, α_{rf} is the roof absorptivity. The absorptivities α_{w} and α_{g} are defined as the effective absorptance of the walls and ground surfaces, respectively. Each one of these terms is calculated by the ratio between the net radiative flux density of the corresponding surfaces and the radiative flux incident on the urban unit:

$$\alpha_{\mathrm{w}} = \frac{1}{K_{\perp}\cos z + D} \sum_{i=1}^{4k} \frac{A_i \Phi_i}{A_{\mathrm{w}}}, \tag{32}$$

$$\alpha_{\mathrm{g}} = \frac{1}{K_{\perp}\cos z + D} \sum_{i=4k+1}^{4k+3} \frac{A_i \Phi_i}{A_{\mathrm{g}}}, \tag{33}$$

where $K_{\perp}$ and D are, respectively, the normal direct and horizontal sky diffuse radiation flux densities (see calculations in Appendix 3), A_{w} and A_{g} are calculated from (29) and (30) and A_i is the area of each sub-surface i. Replacing the Φ_i terms by (6), Eq. (32) becomes the equivalent expression:

$$\alpha_{\mathrm{w}} = \sum_{j=1}^{m} \underbrace{\sum_{i=1}^{4k} \frac{A_i}{A_{\mathrm{w}}} \Psi_{\mathrm{S}i,j}}_{\kappa_{\mathrm{S}}j} \underbrace{\frac{\Omega_{\mathrm{S}}j}{K_{\perp}\cos z + D}}_{\omega_{\mathrm{S}}j}. \tag{34}$$

A similar expression can be obtained for (33). Therefore, the generalized effective absorptance, α_{sf}, for any surface or group of surfaces inside the urban block and formed by n_{sb} subsurfaces, is given by the dot product of two vectors:

$$\alpha_{\mathrm{sf}} = \boldsymbol{\kappa}_{\mathrm{S}} \cdot \boldsymbol{\omega}_{\mathrm{S}} \tag{35}$$

where $\boldsymbol{\kappa}_{\mathbf{S}}$ results from an area-weighting sum of the ψ_{S} lines, corresponding to n_{sb} (36); $\boldsymbol{\omega}_{\mathbf{S}}$ is the irradiation vector normalized by the total urban unit irradiation (37),

$$\kappa_{\mathrm{S}}j = \frac{\sum_{i=1}^{n_{\mathrm{sb}}} A_i \Psi_{\mathrm{S}_{i,j}}}{\sum_{i=1}^{n_{\mathrm{sb}}} A_i}, \tag{36}$$

$$\omega_{\mathrm{Sj}} = \frac{\Omega_{\mathrm{S}}j}{K_{\perp}\cos z + D}, \tag{37}$$

with:

$$\boldsymbol{\Omega}_{\mathbf{S}} = \left(K_1, K_2, \ldots K_{4k+3}, D\right). \tag{38}$$

It is noteworthy that $\boldsymbol{\kappa}_{\mathbf{S}}$ depends only on the urban geometry and surface absorptivity and, therefore, is independent of local solar radiation flux density as well as solar

position. Each component κ_{sj} represents the fraction of the surface j irradiation, which is absorbed by the main surface.

The calculation process for $\mathbf{\Omega}_S$ consists of emitting a set of rays, regularly spaced and with a specific direction (sun direction), and determining the fraction of rays that intersect a surface (see details in Appendix 2), as suggested by Kanda et al. (2005). The $\mathbf{\Omega}_S$ estimation accuracy is proportional to the number of grid nodes, r, which will be discussed in Sect. 5.

The effective absorptance of an urban block depends on the following variables:

$$\alpha_{ub} = f\left[\alpha_{rf},\ urban,\ \boldsymbol{\kappa}_{\mathbf{s}}(urban,\ \boldsymbol{\alpha}),\ \boldsymbol{\omega}(urban,\ \delta,\ climate)\right] \tag{39}$$

where *urban* variables are L_x, L_x, H, W_x and W_x. It is noteworthy that $\boldsymbol{\alpha}$ is a vector because it expresses the absorptivity of all surfaces (α_i), which can take different values. The understanding of the α_{ub} dependence is important when analyzing the influence of different parameters on the urban block absorptance.

4.2 Effective emittance

The emittance of an urban block, ε_{ub}, is defined by the equivalent emissivity of a flat horizontal surface with the same urban unit area (A_{ub}) at an equivalent temperature T_{ub}. To derive an expression for ε_{ub}, first the net longwave radiative flux is defined as:

$$\Phi_L = \varepsilon_{ub}\left(L_\downarrow - \sigma T_{ub}^4\right) A_{ub} \tag{40}$$

where $L_\downarrow$ is the sky downward longwave radiative flux density and σ is the Stephan–Boltzman constant.

It is noteworthy at this point that in a real urban block longwave net radiative flux, Φ_L, is often negative. For example, for a downward radiative flux of 300 W m^{-2}, the longwave radiative flux is negative for surface temperatures above 270 K (−3°C). However, this value increases to 290 K (17°C) if the downward radiative flux is 400 W m^{-2}. Also, if all the surfaces in the urban block are considered, the net longwave radiative flux is calculated from,

$$\Phi_L = \varepsilon_{rf}\left(L_\downarrow - \sigma T_{rf}^4\right) A_{rf} + \sum_{i=1}^{4k+3} A_i \Phi_i. \tag{41}$$

Therefore, from (40) and (41) and using the expression (4) for Φ_i, the urban block emittance is expressed by

$$\varepsilon_{ub} = \varepsilon_{rf}\frac{L_\downarrow - \sigma T_{rf}^4}{L_\downarrow - \sigma T_{ub}^4}\frac{A_{rf}}{A_{ub}} + \left(\sum_{j=1}^{m}\sum_{i=1}^{4k+3} A_i \Psi_{Li,j}\frac{\Omega_{Lj}}{L_\downarrow - \sigma T_{ub}^4}\right)\frac{1}{A_{ub}}. \tag{42}$$

Defining the equivalent temperature equal to the roof temperature and comparing (42) with

$$\varepsilon_{ub} = \varepsilon_{rf}\frac{A_{rf}}{A_{ub}} + \varepsilon_{wg}\frac{A_{wg}}{A_{ub}}, \tag{43}$$

the effective emittance, ε_{wg}, for the group formed by wall and ground surfaces, with $4k + 3$ sub-surfaces and an area A_{wg} equal to the sum of A_w and A_g, is given by the

dot product of the vectors $\boldsymbol{\kappa}_{\mathbf{L}}$ and $\boldsymbol{\omega}_{\mathbf{L}}$ defined, respectively, by

$$\kappa_{\mathrm{L}j} = \frac{\sum_{i=1}^{n_{\mathrm{sb}}} A_i \Psi_{\mathrm{L}i,j}}{\sum_{i=1}^{n_{\mathrm{sb}}} A_i}, \tag{44}$$

$$\omega_{\mathrm{L}j} = \frac{\Omega_{\mathrm{L}j}}{L_{\downarrow} - \sigma T_{\mathrm{rf}}^4}, \tag{45}$$

with:

$$\boldsymbol{\Omega}_{\mathbf{L}} = \left(\sigma T_1^4, \sigma T_2^4, \ldots, \sigma T_{4k+3}^4, L_{\downarrow}\right). \tag{46}$$

The effective emittance of an urban block is a function of *urban* variables, surfaces emissivity vector ($\boldsymbol{\varepsilon}$), surfaces temperature (T_i) and sky downward longwave radiative flux ($L_{\downarrow}$):

$$\varepsilon_{\mathrm{ub}} = f\left[\varepsilon_{\mathrm{rf}},\ urban,\ \boldsymbol{\kappa}_{\mathbf{L}}(urban,\ \boldsymbol{\varepsilon}),\ \boldsymbol{\Omega}(T,\ L_{\downarrow})\right]. \tag{47}$$

In order to obtain surface temperatures, an energy balance model is needed, because these depend not only on the radiative balance but also on convective and conductive heat transfer. However, to simplify this approach, it is assumed that the temperature is constant for all of the wall, ground and roof surfaces. The $\boldsymbol{\omega}_{\mathrm{L}}$ vector takes the form

$$\boldsymbol{\omega}_{\mathrm{L}} = \frac{1}{\left(L_{\downarrow}/\sigma T^4\right) - 1}\left(1, 1, \cdots, 1, \frac{L}{\sigma T^4}\right) \tag{48}$$

and $\varepsilon_{\mathrm{wg}}$ can be simplified to

$$\varepsilon_{\mathrm{wg}} = \frac{1}{\left(L_{\downarrow}/\sigma T^4\right) - 1}\left(\underbrace{\sum_{j=1}^{m-1} \boldsymbol{\kappa}_{Lj}}_{b} + \underbrace{\boldsymbol{\kappa}_{Lm}}_{a}\frac{L}{\sigma T^4}\right) \tag{49}$$

This assumption, even if it is realistic only for certain conditions such as the early morning hours, can be used to characterize the influence of geometry on the effective emittance of the urban block. Further analysis would be required in order to integrate surfaces thermal differences in $\varepsilon_{\mathrm{ub}}$.

The term b, which corresponds to the sum of the $m-1$ terms of $\boldsymbol{\kappa}_{\mathbf{L}}$, is equal to the symmetric of a ($b = -\kappa_{\mathrm{L}m}$). This can be physically explained by the thermal equilibrium among surfaces (T is assumed constant) and the longwave radiative exchanges do occur only between each surface and the sky surface (m). So, rearranging Eq. (49) $\varepsilon_{\mathrm{wg}}$ is given by

$$\varepsilon_{\mathrm{wg}} = \kappa_m. \tag{50}$$

The interpretation of (50) suggests that $\varepsilon_{\mathrm{ub}}$, assuming isothermal conditions, is strictly dependent on the geometry and surface emissivity. For longwave radiation, $\kappa_{\mathrm{L}m}$ represents the fraction of the sky downward longwave radiation flux that contributes to the net radiative flux of the urban block surfaces.

Table 1 Invariant model parameters

Block dimensions	H	15 m
	A_{rf}	225 m^2
Surface properties	α_{w}	0.50
	α_{g}	0.80
Normal direct radiation flux density as a function of zenith angle [$\mathrm{W\,m^{-2}}$]	$K_{\perp(20°)}$	837
	$K_{\perp(40°)}$	763
	$K_{\perp(60°)}$	597
Horizontal sky diffuse radiation flux density [$\mathrm{W\,m^{-2}}$]	D	120

Table 2 Variability of model parameters

Ratio of block dimensions	L_x/L_y	1, 2, 4 and 8
Canyon-aspect ratio	H/W_x	0.5, 1, 2 and 4
	H/W_y	0.5, 1, 2 and 4
Solar zenith [deg]	z	20, 40 and 60
Layout azimuth [deg]	δ	0, 30, 60 and 90

The shape factor between the urban block and the sky, commonly designated by a sky-view factor, can be estimated by calculating $\varepsilon_{\mathrm{ub}}$ for an urban block with black surfaces ($\varepsilon_i = 1$) affected by an area correction factor $A_{\mathrm{ub}}/(A_{\mathrm{ub}} + A_{\mathrm{w}})$. Thus, the effective emittance of an urban block is related to the sky-view factor, which indicates the natural cooling capacity of an urban block relative to its surrounding environment.

5 Matrix approach and ray-tracing method

5.1 Model parameters

The urban block effective absorptance was analytically calculated and compared with the results obtained by a ray-tracing method, hereafter RTM (see details in Appendix 4). The invariant model parameters are synthesized in Table 1, while Table 2 shows the variability of model parameters, using results from 768 different cases. The urban canyon ratio (H/W_x or H/W_x) ranges from the widest (0.5) to the narrowest (4); the block ratio dimensions (L_x/L_y) varied from 1 (a square) to 8 (a cross-sectional long rectangular block). The sun position ranged between high (zenith 20°) and low altitudes (zenith 60°) with azimuth angles of 0° (a, b and c surfaces of Fig. 4 are totally shaded), 30° or 60° (a and c surfaces are totally shaded), and 90° (a, c and d surfaces are totally shaded), Due to surface absorptivity being constant for all surfaces, angles greater than 90° reproduce one of the above solar azimuth positions.

The influence of the simulation parameters — the number of divisions for vertical surfaces k, the number of iterations for shape-factor matrix calculation n_{it}, the number of neighbouring urban units n and the number of grid nodes r to calculate the direct surface irradiation vector ($\mathbf{\Omega}_{\mathrm{S}}$) — was studied using the Pearson correlation coefficient, ρ, obtained by correlating the results of the two methods: RTM and RAM-MC.

Table 3 Analysis of r and k simulation parameters on the Pearson correlation coefficient between radiosity method optimized by Monte Carlo (RAM-MC) and ray-tracing method (RTM) ($n = 10$, $n_{it} = 500$)

ρ		r				
		100	900	2500	4900	10000
k	1	0.879	0.973	0.978	0.976	0.979
	9	0.920	0.989	0.994	0.996	0.997
	25	0.923	0.989	0.996	0.997	0.998
	225	0.916	0.989	0.996	0.997	0.997

Table 4 Analysis of n_{it} and k simulation parameters on the Pearson correlation coefficient between radiosity method optimized by Monte Carlo (RAM-MC) and ray-tracing method (RTM) ($n = 10$, $r = 2500$)

ρ		n_{it}				
		20	50	200	500	5000
k	1	0.879	0.938	0.978	0.978	0.981
	9	0.969	0.985	0.991	0.994	0.996
	25	0.972	0.988	0.994	0.996	0.997
	225	0.972	0.988	0.994	0.996	0.997

Table 5 Analysis of n and k simulation parameters on on the Pearson correlation coefficient between radiative matrix approach optimized by Monte Carlo and ray-tracing method ($n_{it} = 500$, $r = 2500$)

ρ		n				
		1	2	4	10	30
k	1	0.224	0.760	0.979	0.978	0.978
	9	0.269	0.790	0.994	0.994	0.994
	25	0.275	0.789	0.995	0.996	0.996
	225	0.279	0.794	0.995	0.996	0.996

5.2 Results

From the sensitivity analysis of the Person correlation coefficient ρ to the simulation parameters, we conclude that increasing the number of grid nodes r improves the value of ρ, independently of the value chosen for k (Table 3). However, no significant improvements were verified for r higher than 2500. A larger number of subdivisions, k, also increases ρ (Tables 3–5), to a limit of 25, above which no further improvements in ρ are observed. The n parameter depends on the correlation between results, and should be at least higher than 4 (Table 5). In terms of the n_{it} parameter, a better correlation is obtained for values higher than 500 (Table 4). It is noteworthy that higher values of the simulation parameters increase the calculation time; moreover, for time step calculations an increase of r increases significantly the calculation time. From this sensitivity analysis, it can be concluded that the simulation parameters n_{it} and n have a minor effect on the results, so long as they are set higher than 500 and 4, respectively. The selection of k and r should be established according to a best-accuracy versus time-calculation cost criterion.

For k, r, n_{it} and n equal to 25, 2500, 500 and 10, respectively, RAM-MC produces α_{ub} values that are better correlated with RTM (ρ is 0.996), as shown in Fig. 7. The maximum difference between RAM-MC and RTM is less than 2%. The advantage of RAM-MC is in the smaller CPU time used to perform calculations. For example, a total number of 768 cases is calculated in less than one hour of CPU time, against more than 36 h of calculation when RTM is used. These differences are mainly due to the fact that, for each geometry, RAM-MC calculates once only the shape-factor matrix

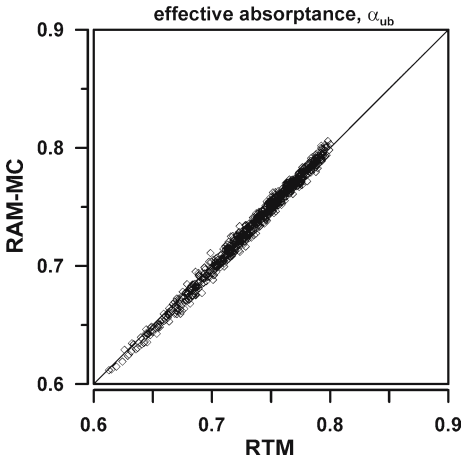

Fig. 7 Effective absorptance calculated by the radiosity method optimized by Monte Carlo (RAM-MC) and ray-tracing method (RTM)

and does not need to repeat the inter-reflection process. Besides the $\mathbf{\Omega}_S$ calculation, no other iterative processes are performed for different sun positions. Therefore, because the geometry is invariant, RAM-MC is strongly recommended for repeated timestep calculations of the net radiative fluxes during long periods.

6 Matrix approach and experimental results

The urban block effective absorptance calculated by the method described in Sect. 4.1, using the urban shortwave matrix methodology, is compared with the measurements of Aida (1982) for three urban layouts defined for model 1 (north–south street), 2 (east–west street), and 3 (blocks). The experiment consisted of measuring hourly urban albedo for a set of small concrete blocks. The measurements provided by Aida (1982) show that the absorptivity of a flat concrete surface is correlated with the zenith angle, in radians, by

$$\alpha_{\text{concrete}} = \begin{cases} 0.64 - 0.06z^2, & z \le \pi/3 \\ 0.59 - 0.01z^8, & z > \pi/3 \end{cases} . \tag{51}$$

In the model the reflections are assumed perfectly isotropic due to the fact that RAM-MC is based on shape-factor geometry and does not distinguish between first and higher order reflections. In order to integrate the variation of the surface absorptivity with the angle of incidence applied mainly to direct radiation incidence, in the model validation, only the absorptivity of the unshaded horizontal surfaces is calculated from (51). The absorptivity of the remaining surfaces is set to 0.64. This assumption introduces an error on the urban albedo estimation, because the surface absorptivity of unshaded surfaces is underestimated for second- and higher-order inter-reflections. The direct and diffuse solar radiation data are calculated for each one of the Julian days (model 1: 208, model 2: 209, model 3: 173) following the methodology described in Appendix 3. The model parameters k, r, n_{it} and n are set to 100, 10000, 2000 and 10, respectively.

Generally, RAM-MC adequately reproduces the measurements for all urban layouts, as shown in Fig. 8.

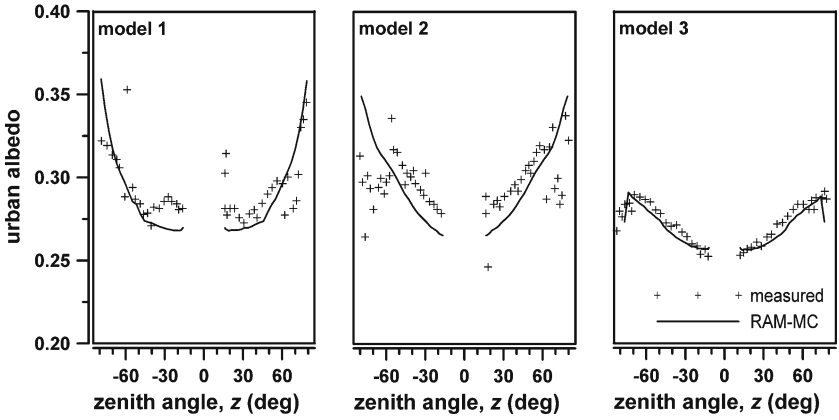

Fig. 8 Hourly urban albedo: comparison between radiosity method optimized by Monte Carlo (RAM-MC) and measurements (adapted from Aida 1982): (1) north–south street, (2) east–west street and (3) blocks

7 Sensitivity studies

7.1 Urban block effective absorptance

The influence on the urban block effective absorptance of different geometrical parameters of the urban layout is analyzed by the ratios: H/W and $H/(W + L)$, fixing the distance among blocks, $W = 15$, and varying the building height, H, and the block width, L, for each of the directions x and y. The effective absorptance is calculated for the summer and the winter solstice days, 172 and 355 Julian day, respectively, at 20°, 40° and 60° latitude, considering the daily integration of the different hourly sun positions. Walls, roof and floor absorptivities are assumed equal to 0.5.

7.1.1 The canyon aspect ratio

The effective absorptance is obtained for the following urban layouts: square blocks, i.e. square cross-sectional blocks (Fig. 9a); rectangular blocks, i.e. rectangular cross-section blocks (Fig. 9b); and street, i.e. long rectangular cross-sectional blocks that approximate an infinite street (Fig. 9c). These cases are characterized by L equal to W, $3W$ and $15W$, respectively. Rectangular blocks and street configurations have two possible orientations: forming an east–west street (EW) or a north–south street (NS). The canyon-aspect ratio, H/W, ranges from 0.5 to 4 with 0.5 discrete steps (Fig. 10).

From the results of the sensitivity study it can be concluded that the effective absorptance increases with the canyon-aspect ratio of the urban layout, H/W, as depicted in Fig. 11a, b. For square blocks with H/W equal to 1, the effective absorptance is increased about 30% (both in summer and winter days), when compared to a flat surface absorptivity. The square block is the urban configuration that absorbs more solar radiation, followed by the rectangular block layout and, finally, the street configuration. In terms of block orientation, the effective absorptance is higher for an east–west street than for a north–south street in summer (Fig. 11a). This difference is,

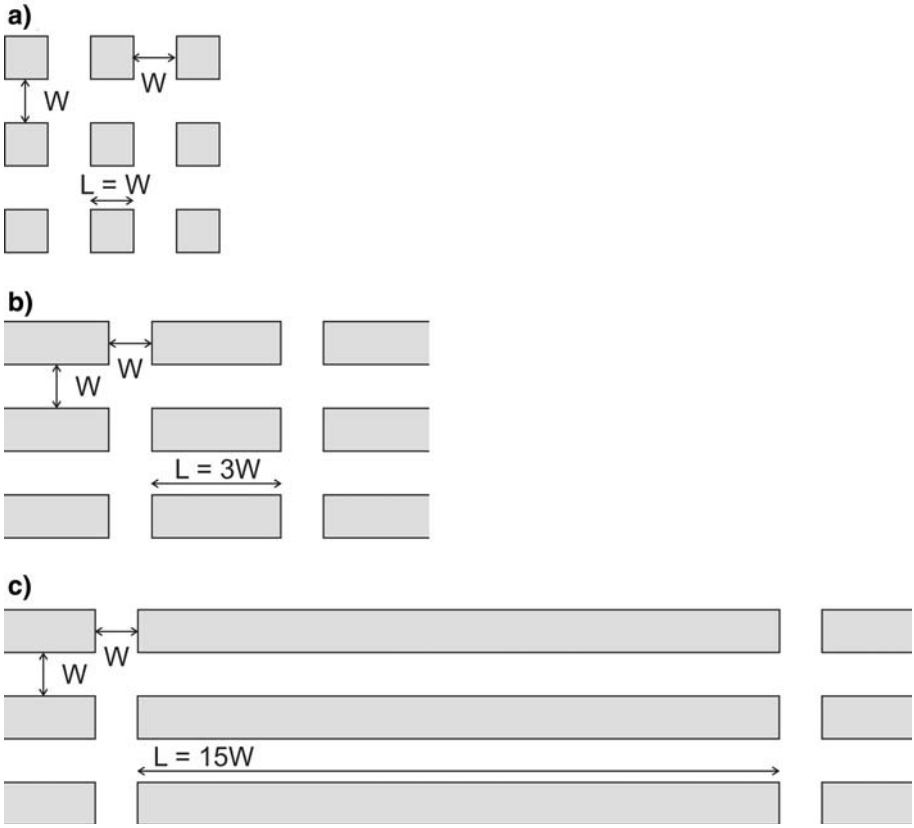

Fig. 9 Urban layout cases: (**a**) square cross-section blocks, (**b**) rectangular cross-sectional blocks, and (**c**) street

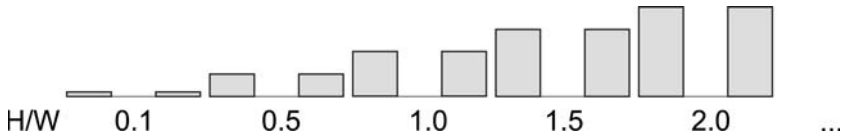

Fig. 10 Variability of canyon-aspect ratio

however, negligible for higher latitudes (60°). In winter, the north–south layout has a higher effective absorptance (Fig. 11b).

7.1.2 Urban structure: square blocks to street layout

The study is repeated fixing the canyon-aspect ratio of the urban layout at 0.5, 1, 1.5 and 3. The ratio $H/(W + L)$ is decreased, by increasing the width block, L, with increments in W, in order to have geometries where L corresponds to l times W. For example, l takes the value of 1 for square blocks (Fig. 9a) and 3 for rectangular blocks (Fig. 9b). For all cases, l ranges between 1 and 15. So long as $H/(W + L)$ decreases (l increases), the effective absorptance of the urban layout converges to the

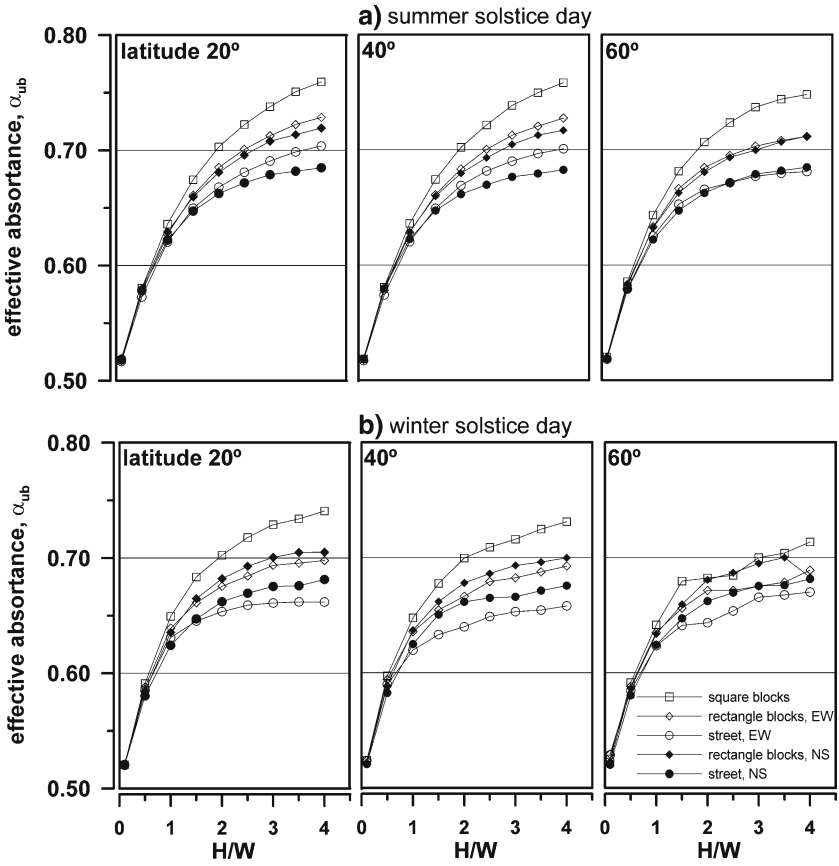

Fig. 11 Variability of effective absorptance with canyon-aspect ratio, (**a**) for summer, and (**b**) winter solstice days

absorptance of an infinite street. The approximation of a specific geometry for the equivalent bi-dimensional infinite street varies with the latitude and the urban layout geometry. For all the tested cases the convergence is obtained for $l \geq 11$, using, as a convergence criterion, that the difference between values of the flat surface absorptance is below 1%. The values of l for each one of the cases are indicated in the Fig. 12, where the latitude is fixed at 40°.

7.2 Urban block effective emittance

The effective emittance also increases with the canyon-aspect ratio as shown in Fig. 13. For the square block layout with H/W equal to 1, this increase is about 8% when compared to a flat surface emissivity. It is noteworthy that, despite the trapping effect of emitted radiation, the increase of the urban block emittance results from a higher transference surface area of the urban structure compared to a flat surface. As a consequence, the square block layout has a higher effective emittance than the remaining configurations (Fig. 13).

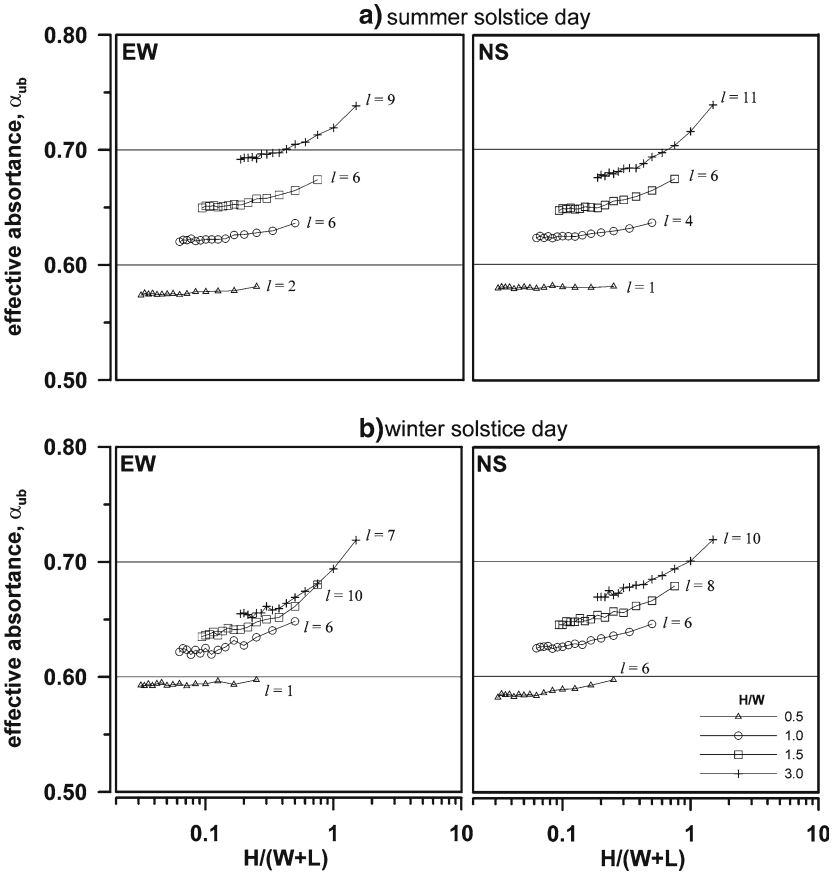

Fig. 12 Variability of effective absorptance with urban layout, (**a**) for summer, and (**b**) winter solstice days

Fig. 13 Variability of effective emittance with urban layout

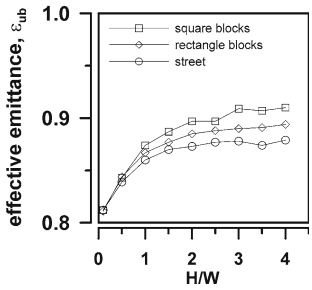

8 Conclusions

The methodology presented combines the exact solution obtained by solving a set of linear equations (matrix formulation) with Monte Carlo techniques to estimate the net radiative balance on the surfaces of an urban structure. The reason for coupling Monte Carlo techniques is due to the complexity associated with shape-factor

calculations, via analytical equations, for a 3D geometry with variations on building and street dimensions on both x- and y-axes. The results obtained are validated by experimental data and are well correlated with those calculated by the ray-tracing method, with the advantage of reducing by a factor of 36 the time used to perform calculations. The large reduction of the CPU time allows application of this method to timestep calculations of net radiative balance for long periods and, therefore, the method can be integrated on urban canopy-layer models.

From the results of the sensitivity study it can be concluded that the effective absorptance increases with the canyon-aspect ratio of the urban layout, independently of the latitude and the season, as well as the effective emittance. An urban structure formed by square cross-sectional blocks absorbs more solar radiation than an urban structure formed by rectangular cross-sectional blocks. The street layout is the configuration that absorbs least solar radiation. For the summer solstice day, north–south orientation of the rectangular blocks causes a lower effective absorptance; on the other hand, for the winter solstice day, the same orientation results in a higher effective absorptance. The approximation of a specific geometry for an equivalent bi-dimensional infinite street can be applied for rectangular cross-sectional blocks, where the width is 11 times more than the depth dimension. For some specific cases that proportion can be reduced.

Acknowledgements The authors acknowledge the contribution of the Portuguese National Foundation of Science and Technology of the Ministry for Science and Technology by supporting Marta J. N. Oliveira Panão with a PhD Grant (SFRH/BD/12256/2003).

Appendix 1: Shape-factor matrix calculation

The estimation of the shape-factor matrix **F** is based on ray tracing by sending a large amount of rays, n_{it}, from each surface with random direction, and tracking which surfaces they intersect (Kondo et al. 2001). Each term of the **F** matrix, $F_{i,j}$, is the fraction of rays arriving from surface i that intersects surface j. Because the urban layout is formed by a large number of urban units, and the shape-factor terms include all the surfaces a, b, c and d of the neighbouring units, when a ray exits the urban unit from a certain surface, another ray re-enters from the opposite side. This operation is repeated n times, which means that the shape factors include the surfaces of the $n-1$ neighbouring urban units.

Because some surfaces are similar in terms of geometric dimensions and position, namely a is similar to b, and c similar to d, the ray tracing is applied only once and the shape-factor matrix is updated accordingly. This iterative process was implemented on MATLAB. The selection of the simulation parameters, n_{it} and n, is discussed in Sect. 5.

Appendix 2: $\Omega_{\mathbf{S}}$ calculation

For a 3D model, the estimation of shading and sunlit patterns of each surface is quite complex. For the present model, the direct irradiance of each surface, K_i, is estimated by considering that direct solar energy incident on the urban unit top surface is redistributed among all the surfaces of an urban unit, in order to consider the corresponding inhomogeneities. Accordingly, K_i is expressed by

$$K_i = \frac{\mathrm{f}_i K_\perp \cos z \,(L_x + W_x)\,(L_y + W_y)}{A_i} \tag{52}$$

where A_i is the surface area, z is the zenith angle and $K_\perp$ is the normal direct radiation flux density (see calculations in Appendix 3). The f_i term corresponds to the fraction of the total energy incident on surface i, which is evaluated from the fraction of rays sent from the horizontal top surface that intersects the surface. The rays are regularly spaced and form a grid with r nodes; their direction corresponds to that of the sun's and is a function of the solar zenith and azimuth angles. The selection of the number of grid nodes, r, is discussed in Sect. 5 and the iterative process of sending rays was implemented on MATLAB and has a formulation similar to that described in Appendix 1.

Appendix 3: Direct and diffuse irradiances

The global and normal direct irradiances, G and $K_\perp$, take into consideration the Linke turbidity factor T_L (Linke 1922) and air mass (M), according to Perrin de Brichambaut and Vauge (1982) and Kasten (1980), respectively. The diffuse irradiance, D, is calculated thus, viz.

$$G = r_{\mathrm{se}} I_0 \,(0.929 - 0.041 T_{\mathrm{L}}) \cos z^{\frac{T_{\mathrm{L}}+36}{33}}, \tag{53}$$

$$K_\perp = r_{\mathrm{se}} I_0 \,\exp\left(\frac{-M.T_{\mathrm{L}}}{0.9M + 9.4}\right), \tag{54}$$

$$D = G - K_\perp \cos z, \tag{55}$$

where I_0 is the solar constant (1367 W m^{-2}), and r_{se}, the sun–earth distance factor, is calculated for the specific Julian day, J_{day}, from

$$r_{\mathrm{se}} = 1 + 0.034 \cos(0.986 J_{\mathrm{day}} - 2). \tag{56}$$

For large urban areas T_L is taken as 4.5 (Bourges 1992). For each zenith angle z, the air mass is estimated according to:

$$M = \frac{1 - 0.1h}{\cos z} \tag{57}$$

where h is the altitude above sea (0.2 km).

Appendix 4: Ray-tracing method

The ray-tracing method applied to the 3D structure is a process very similar to that described for the shape-factor calculation. However, a test is performed each time a ray intersects a surface, in order to determine if it is absorbed or reflected. When a diffuse reflection occurs a new direction is randomly determined. In this case, no specular reflections are considered. This process is repeated for a large number of rays, until the fraction of rays absorbed by the urban block converges. The convergence criterion consists of keeping the residual value in the last 1,000 iterations below 0.01.

References

Aida M (1982) Urban Albedo as a function of the urban structure — a model experiment. Boundary-Layer Meteorol 23:405–413

Arnfield AJ (1982) An approach to the estimation of the surface radiative properties and radiation budgets of cities. Phys Geog 3:97–122

Arnfield AJ (1988) Validation of an estimation model for urban surface Albedo. Phys Geog 9:361–372

Arnfield AJ (2003) Two decades of urban climate research: a review of turbulence, exchanges of energy and water, and the urban heat island. J Climat 23:1–26

Athienitis AK Santamouris M (2002) Thermal analysis and design of passive solar buildings. James & James, London, 288 pp.

Bourges B (1992) Climate data handbook for Europe. Kluwer Academic Publishers, London, 112 pp.

Chimklai P, Hagishima A, Tanimoto J (2004) A computer system to support albedo calculation in urban areas. Building Environ. 39:1213–1221

Harman IN, Best M, Belcher S (2004) Radiative exchange in an urban street canyon. Boundary-Layer Meteorol 110:301–316

Johnson GT, Watson ID (1984) The determination of view-factors in urban canyons. J Climate Appl Meteorol 23:329–335

Kanda M, Kawai T, Nakagawa K (2005) A simple theoretical radiation scheme for regular building arrays. Boundary-Layer Meteorol 114:71–90

Kasten F (1980) A simple parameterization of two pyrheliometric formulae for determining the Linke turbidity factor. Meteorol Res. 33:124–127

Kawai T, Kanda M (2003) Three dimensional radiation model for urban canopy. J Hydrol Eng 47:55–60 (in Japanese)

Kobayashi T, Takamura T (1994) Upward longwave radiation from a non-black urban canopy. Boundary-Layer Meteorol 69:201–213

Kondo A, Ueno M, Kaga A, Yamagushi K (2001) The influence of urban canopy configuration on urban Albedo. Boundary-Layer Meteorol 100:225–242

Kusaka H, Kondo H, Kiregawa Y, Kimura F (2001) A simple single-layer canopy model for atmospheric models:comparison with multi-layer and slab models. Boundary-Layer Meteorol 101:329–358

Linke F (1922) Transmissions-Koeffizient und Trübungsfaktor. Beitr Phys fr Atmos 10:91–103

Martilli A, Clappier A, Rotach MW (2002) An urban surface exchange parameterization for mesoscale models. Boundary-Layer Meteorol 104:261–304

Masson V (2000) A physically-based scheme for the urban energy budget in atmospheric models. Boundary-Layer Meteorol 94:357–397

Mills GM (1993) Simulation of the energy budget of an urban canyon — I. Model structure and sensivity Test. Atmos Environ 27B:157–170

Nunez M, Oke T (1977) The energy balance of an urban canyon. J Appl Meteorol 16:11–19

Pawlak W, Fortuniak K (2002) Estimation of the effective Albedo of the urban canyon – comparison of two algorithms. Proceedings of the international conference man and climate in the 20th Century. Wroclaw, Poland

Pawlak W, Fortuniak K (2003) Application of physical model to study effective Albedo of the urban canyon. Proceedings of the fifth international conference on urban climate. Lodz, Poland

Perrin de Brichambaut C, Vauge C (1982) Le gisement solaire: Evaluation de la ressource énergétique. Technique et documentation, Lavoisier, Paris

Sakakibara Y (1996) A Numerical study of the effect of urban geometry upon the surface energy budget. Atmos Environ 30:487–496

Santamouris M (2001) Energy and climate in the urban built environment. James & James, London, 402 pp.

Sparrow EM, Cess RD (1978) Radiation heat transfer, Hemisphere Publishing Corporation, Washington, DC, 306 pp.

Steyns DG, Lyons TJ (1985) Comment on the determination of view-factors in urban canyons. J Climate Appl Meteorol 24:383–385

Swaid H (1993) The role of radiative-convective interaction in creating the microclimate of urban street canyons. Boundary-Layer Meteorol 64:231–259

Verseghy DL, Munro DS (1989a) Sensitivity studies on the calculation of the radiation balance of urban surfaces: I. Shortwave radiation. Boundary-Layer Meteorol 46:309–331

Verseghy DL, Munro DS (1989b) Sensitivity studies on the calculation of the radiation balance of urban surfaces: II. Longwave radiation. Boundary-Layer Meteorol 48:1–18

Yoshida A, Tominaga K, Watani S (1990–91) Field measurements on energy balance of an urban canyon in the summer season. Energ. Buildings 15–16:417–423